An Experimental Study on Harmonic Drives

Technical Report Submitted to

International Submarine Engineering Ltd.

Port Coquitlam, BC, V3C 2M8

H.D. Taghirad, P.R. Belanger, and A. Helmy

Center for Intelligent Machines,
McGill University, 3480 University St.,
Montréal, PQ, H3A 2A7

March 1, 1996

Contents

List of Figures

List of Tables

Abstract

Despite widespread industrial application of harmonic drives, modelling and control of such systems has not been fully addressed. In this theoretical/experimental study of harmonic drive systems a systematic way to capture and rationalize the dynamics of the system is proposed. Simple and accurate models for their compliance, hysteresis, and friction are given and model parameters are estimated from experimental data using least square approximation. A statistical measure of consistency is defined, by which the reliability of the estimated parameter for different operating condition, as well as the accuracy and integrity of the proposed model is quantified. The validity of the modelling scheme is evaluated by comparing the experimental and simulation results. Two separate simulations are developed for the harmonic drive system operating in restrained and unrestrained motion.

The problem of torque control of harmonic drive is addressed in the $\mathcal{H}_\infty$ controller design framework. It has been shown that an empirical nominal model estimated from system frequency responses, provides necessary requirements for controller design. It is illustrated that $\mathcal{H}_\infty$ framework is a very rich and powerful theory to ensure the stability and performance in the presence of modelling uncertainties. An $\mathcal{H}_\infty$ torque controller is implemented on the system, and the time and frequency domain performances of the closed loop system are shown to be exceptionally good.

1 Introduction

Since its inception in 1955, the harmonic drive has found widespread acceptance among practitioners. This mechanical transmission, occasionally called "strain-wave gearing", employs a continuous deflection wave along *non-rigid gear* to allow for gradual engagement of gear teeth (Figure 1). Because of this unconventional gear-tooth meshing action, harmonic drives can deliver high reduction ratios in a very small package. In fact, the radical mechanical operation of this gear train defies conventional understanding of gear behaviour and creates a new arena for exploration and understanding.

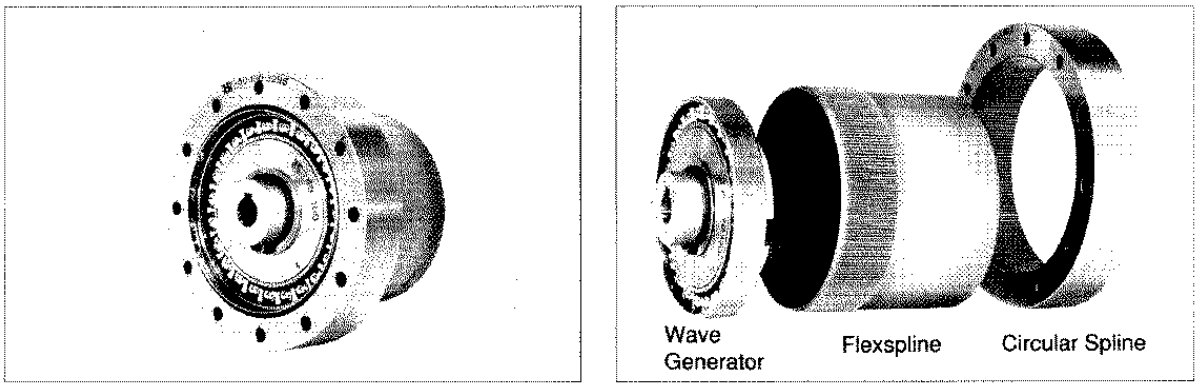

Figure 1: Harmonic drive components

The harmonic drive exhibits performance features both superior and inferior to conventional gear transmissions. Its performance advantages include high torque capacity, concentric geometry, lightweight and compact design, zero backlash, high efficiency, and back drivability. Harmonic drive systems suffer however, from high flexibility, resonance vibration, friction and structural damping nonlinearities. The lack of literature, relative to that for conventional gear transmission also inhibit their use.

The unique performance features of the harmonic drive have captured the attention of designers in many fields. It has been used in industrial and space robots, assembly equipment, and measuring instruments, as well as heavy duty applications such as machine tools and printing presses. Additionally, space and aircraft systems often employ harmonic drives for their light weight and compact geometry. However, the performance disadvantages of harmonic drive motivates the ongoing research on better understanding of the harmonic drive systems, and finding control schemes which reduce the unwanted dynamics.

In many application specifically in robotics, torque is often taken to be the control input. The physical variable being manipulated, however, is not torque but armature current in a DC motor, for instance. For harmonic drive systems the relation between output torque and input current possess nonlinear dynamics, due to the flexibility, Coulomb friction and structural damping of harmonic drive. The main objective of this research is to improve this input/output relation through compensation for nonlinearities, and to convert the system to a torque source with a flat frequency response over a wide bandwidth. Moreover, how accurate we should model the system to obtain a desired performance, is another question to be answered. Finally, we would like to experiment the controller on a single robot arm, whose joint is actuated by harmonic drive, and to

observe its performance in practice.

Throughout its short existence, the harmonic drive has enjoyed increasing international attention from designers as well as researchers. The Russians were perhaps the first who initiated substantial research on the dynamic behavior of harmonic drives [3, 32].

More recently Tuttle and Seering performed an extensive effort to model the stiffness, positioning accuracy, gear tooth-meshing mechanism and friction of the harmonic drive [30, 31]. Their experimental observations show that the velocity response to step commands in motor current are not only contaminated by serious vibration, but also by unpredictable jumps. The velocity response observations were used to guide the development of a series of models with increasing complexity to describe the harmonic drive behavior. Their most complex model included kinematic error, nonlinear stiffness, and gear-tooth interface with frictional losses.

Kircanski and Goldenberg have also attempted to model the harmonic drive in detail [23]. They used the drive system in contact with a stiff environment, in contrast to unrestrained motion experiments used in [31], and illustrated that in this case nonlinear stiffness, hysteresis and friction are more tractable. Simple models for soft-windup, hysteresis, and friction were proposed and the parameters were identified by restrained motion experiments.

Hsia [19], Legnani [24], Marilier [26], and Seyfferth [27] are among others who attempted to model the stiffness, friction, and position accuracy of harmonic drive systems. All these researchers noted the inherent difficulties in finding an accurate model for the system.

Brigdes et al. [9], Kaneko et al. [21], Kazerooni [22], Hogan [18], and Chapel and Su [10] are representative of researchers who worked on the control of harmonic drive system. Bridges [9] used a very simple linear model for the system, with PD torque control. His results show some improvement in tracking error, but insufficient performance near resonant frequency. Kaneko [21], also based his analysis on a simple model of the system, but included nonlinear stiffness in the system. He then applied a feedforward loop to adjust for nonlinear stiffness and then a pure gain torque feedback to shape the performance. Kazerooni [22], considers a simple linear system for the harmonic drive, and used a sensitivity loopshaping technique to design a linear controller for the system. Hogan [18], proposed impedance control for robots with harmonic drive systems, to deal with the dynamic interaction induced in contact tasks. Chapel [10], applied $\mathcal{H}_\infty$control design methods to the analysis and design of impedance control laws.

In this report, first the experimental setup of the harmonic drive is described. Then the results obtained on the system modelling and identification is illustrated, and the fidelity of the model is verified by simulations. The results on robust torque control of system in locked load and free load cases is outlined next, and finally, the report is concluded by the summary of the results and possible future research horizons.

2 Experimental Setup

A picture of the setup and its schematic are illustrated in Figure 2. The harmonic drive is driven by a DC motor, and a load inertia is used to simulate the robot arm for unrestrained motion. Also a positive locking system is designed such that the output load can be locked to the ground. The detail design drawings of the setup are collected in Appendix C. In this experimental setup the flexspline is fixed to the ground and the output is carried by the circular spline.

The DC motor is a brushless Kollmorgen Inland motor model RBE-01503-A00. Its weight is 475 grammes, its maximum rated torque is 5.6 Nm, and its torque constant is 0.1815 Nm/amp.

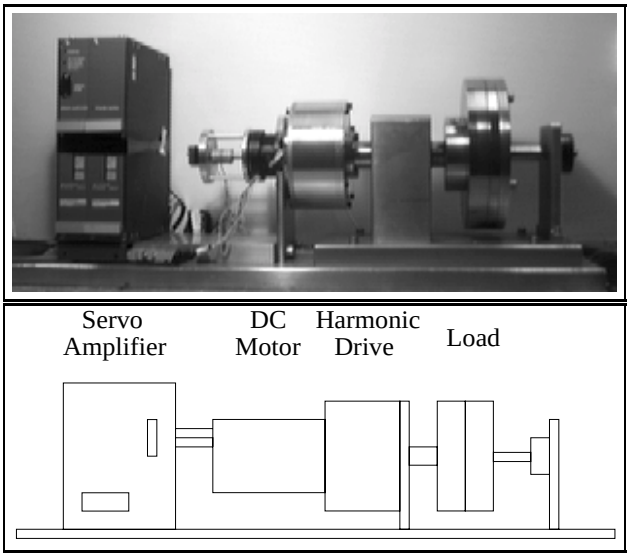

Figure 2: A picture of the experimental setup and its schematics

The servo amplifier is a FAST Drive Kollmorgen, model FD 100/ 5E1. The motor was equipped with a 50 pulse/rev encoder, and the servo amp includes a DSP to estimate the motor velocity from position readings of the encoder. However, the encoder resolution for our low speed experiments was not enough to obtain an accurate estimate of the velocity. Therefore, a tachometer has been purchased form Kollmorgen Inland, and has been replaced the encoder. The detail drawings of the tachometer assembly are given in Appendix C. The harmonic drive is from CFS series of HD Systems, Inc. with gear ratio 160:1, and rated peak torque of 178 Nm. To measure the torque a pair of strain gauges has been mounted on the flexspline by I.S.E., and the output signal is amplified by 1000 using Entran amplifier. We replaced the amplifier to a variable gain amplifier, which has the capability of resetting the offset. The output encoder is Renco model RM21 with 4000 pulse/rev resolution. The technical specification of the system components are collected in Appendix D. Motor velocity and current, and the output torque and position are measured by the measurement units. To obtain an estimate of the output velocity, a Kalman filter estimator on encoder readings [6], is employed. These signals were processed by several data acquisition boards and monitored by a Challenger C–30 processor executing compiled computer C codes.

2.1 Tachometer Calibration

To calibrate the tachometer, we mounted an encoder on the free side of the motor shaft, and experiment the motor for different inputs. The output signal of the tachometer is then, integrated off line in Matlab, and compared to the encoder readings. Using least square approximation for each experiment, we estimate the optimum tachometer gain which best fits the integrated velocity signal and the encoder position signal. Matlab file tach–ls.m given in Appendix A provides the details of the least square approximation. The final gain is obtained from the average value of the estimated gain for different experiments, and the consistency measure of the gain is calculated by the ratio of the standard deviation to the final gain. The final gain is obtained by this method for eight experiments, and the results are given in Table 1. The tachometer gain is 30.05 rad/sec/volts, and the consistency measure is less than 1%, which shows an accurate calibration process.

Tachometer Gain	Consistency measure
30.05	1%

Table 1: Tachometer calibration results

2.2 Torque Sensor Calibration

To experiment the dynamics of the torque sensor and to calibrate it, we locked the harmonic drive wave generator, and applied known torque on the circular spline. The locking device is a simple shaft resembling the motor shaft, which can be fixed to the ground. The detail design drawing of the torque sensor calibration assembly are given in Appendix C. The output torque is applied using arm and weight method. The torque calibration consists of loading and unloading some weight on the arm, in both direction. This experiment is repeated at different circular spline positions, to check the position dependency of the torque sensor. Also low torque and high torque experiments are applied at each position to evaluate the nonlinearity of the torque sensor. Two typical experiment results are shown in Figure 3. The torque sensor gain is obtained using least square approximation, as explained in Section 2.1. The final result is given in Table 2, where the gain is 16.75 Nm/volts, with consistency measure of 3%. This illustrates that the linearity of the torque sensor is good, and it is not position dependent. However, the sensitivity obtained here is 0.6061 volts/Nm, which is almost twice as that reported in I.S.E. report for the same operating condition.

Torque Sensor Gain	Sensitivity volts/Nm	Consistency measure
16.75	0.06061	3%

Table 2: Torque sensor calibration results

3 System Modelling and Identification

The goal of modelling the harmonic drive system is to discover a simple representation which can replicate system performance to a desired level of accuracy. A computer model will be the basis for discovering and examining the proposed control algorithms, before implementing them in practice. Usually a simple model could serve for the controller design purpose. However, in this research a rather complete model of the system is created to aid understanding of the system. In practice it has been proven that the knowledge obtained through the process of modelling and identification of the system becomes a powerful medium for understanding, and improving the design, as well as providing new horizons for controller design.

3.1 DC–Motor Characteristics

A DC motor can be viewed as a two input, one output black box, where the servo amplifier current and external torque are the inputs and the angular displacement (or velocity) is the output.

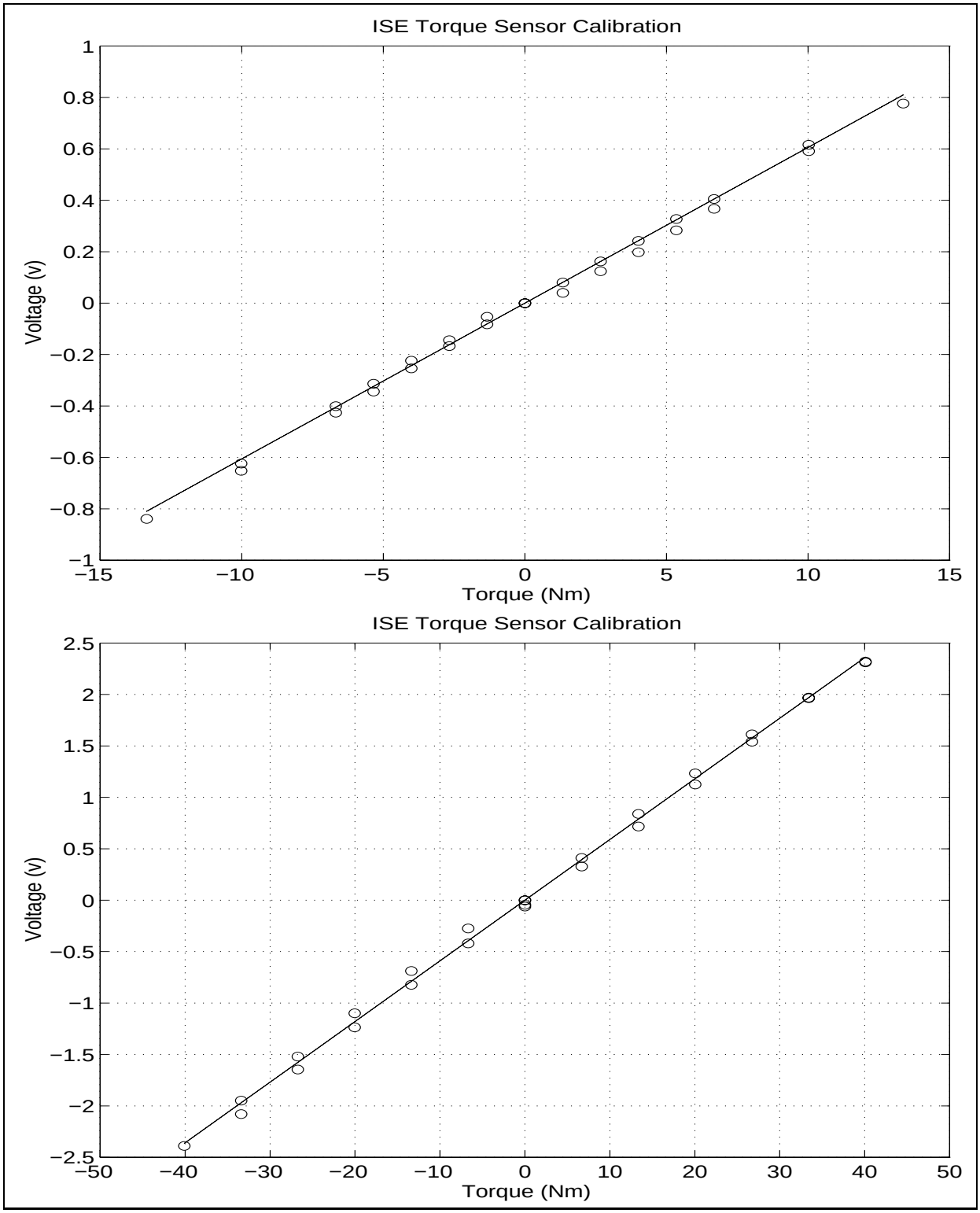

Figure 3: Torque sensor calibration results for low and high torques

	Estimated Parameter	Consistency Measure
K_m	0.1815	0%
J_m	5.8×10^{-5}	5.75%
T_{v_p}	8.6×10^{-4}	7.75%
T_{v_n}	5.8×10^{-4}	14.4%
T_{s_p}	1.5×10^{-2}	25.9%
T_{s_n}	2.7×10^{-2}	25.8%

Table 3: DC motor estimated parameters

The torque balance for the DC motor can be written in the form:

$$K_m i = J_m \ddot{\theta} + T_{f_m} + T_{out} \tag{1}$$

where K_m is the motor torque constant, i is the input current to the motor, J_m is the motor inertia, and T_{out} is the external torque. T_{f_m} is the friction torque, which can be modelled in the form of velocity direction dependent viscous and Coulomb friction as follows:

$$T_{f_m}(\dot{\theta}) = T_{v_n} u_{-1}(-\dot{\theta})\dot{\theta} + T_{v_p} u_{-1}(\dot{\theta})\dot{\theta} + T_{s_n} u_{-1}(-\dot{\theta})\text{sign}(\dot{\theta}) + T_{s_p} u_{-1}(\dot{\theta})\text{sign}(\dot{\theta}) \tag{2}$$

where

$$u_{-1}(x) = \begin{cases} 1 & \text{if } x > 0 \\ 0 & \text{if } x \leq 0 \end{cases} \tag{3}$$

Note that the indices p and n represents the dependence of the friction coefficients on the velocity direction.

The model parameters are estimated by least square approximation. Using Equation 1 as a linear regression model, and measuring the motor velocity and current for two sets of high and low velocity experiments, the model parameters can be estimated using *Moore–Penrose generalized inverse* [13, 8]. Householder reflection is utilized in numerical calculations to avoid ill conditioning [16].

By means of least square estimation, for each experiment we obtained a set of parameters. However, these parameters are deemed acceptable, only if they are consistent for other experiments. By consistency we mean a statistical measure, namely the ratio of the standard deviation to the average value of each parameter estimated for different experiments. If this measure is small, we have a good consistency for different experiments, and in other words, the model is good enough to capture the dynamics of the system.

Figure 4 illustrates the velocity fit obtained by the model for two typical experiments. The model is capable of capturing the dynamics of the system for both low and high velocity experiments. Table 3 summarizes the estimation results for the DC–motor obtained from 15 experiments, in which the values of parameter are expressed in SI units. Note that the motor torque constant K_m from the motor specs assumed to be known in the least square estimation. The consistency measure of the results for different experiment shows less than 15% for some parameters, and less than 30% in others. The reason for variation in consistency measure among parameters is that some experiments are not persistently exciting to estimate those friction coefficients. However, it has been verified by simulations that having consistency measure less than 30% gives relatively good match to the experiments. For details of the approximations you can refer to file mot–ls.m given in Appendix A.

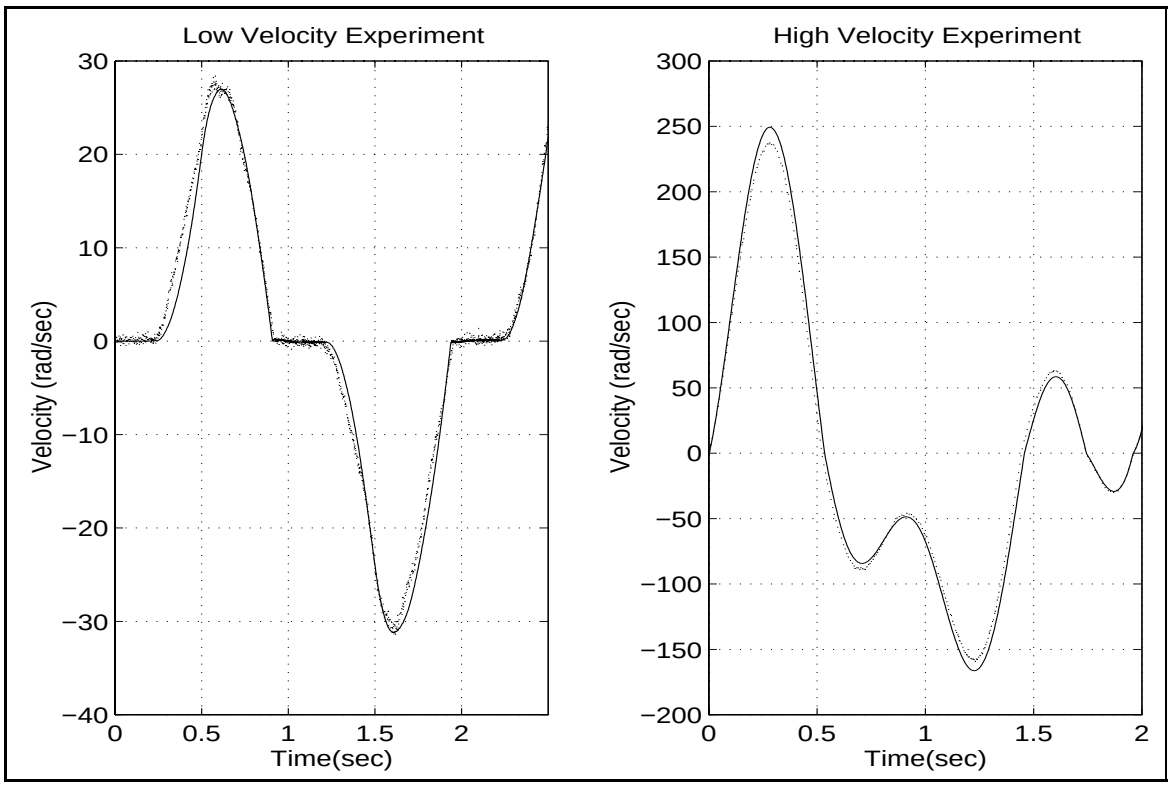

Figure 4: Velocity comparison of the model and experiment for two typical experiments

3.2 Servo Amplifier Characteristics

The servo amplifier has been modelled next. Servo amplifier acts as a current source when the motor is operating at low speeds/high torques. However, it has been observed that this is not the case when motor is working at high speeds. The main reason for this is the back EMF effect of the motor. To capture the dynamics of the servo amp for these two operating regimes, first the system in locked load case has been experimented. The frequency response of the system has been obtained using DSP Technology Inc., Siglab hardware [1]. The system response is illustrated in Figure 5, which is flat up to 300 Hz, and the transfer function of the system can be approximated by :

$$\frac{\text{Current}}{\text{Ref Voltage}} = \frac{2.48 \times 10^9 (s - 2593.9 \pm j3032.6)}{(s + 732)(s + 856.1 \pm j3437.0)(s + 1134.4 \pm j1661.3)} \tag{4}$$

For low frequency applications, however, its DC-gain $k = -1.0653$ as a pure gain is a sufficiently good model. The Matlab code used to approximate the transfer function of the system is amp–freq–fit.m which is given in Appendix A.

The behavior of the system at higher speeds has been analyzed using free load experiments. A series of frequency responses of the system with different reference voltage amplitude is experimented, and the results are illustrated in Figure 5. As the motor speed increases the DC gain of the servo amplifier decreases. For maximum speed of the system the DC gain will reduces to -0.2, and for nominal operating speed of the motor it reduces to -0.5155. For low frequency application, a simple gain $k = -0.5155$ is used to simulate the servo amplifier behavior.

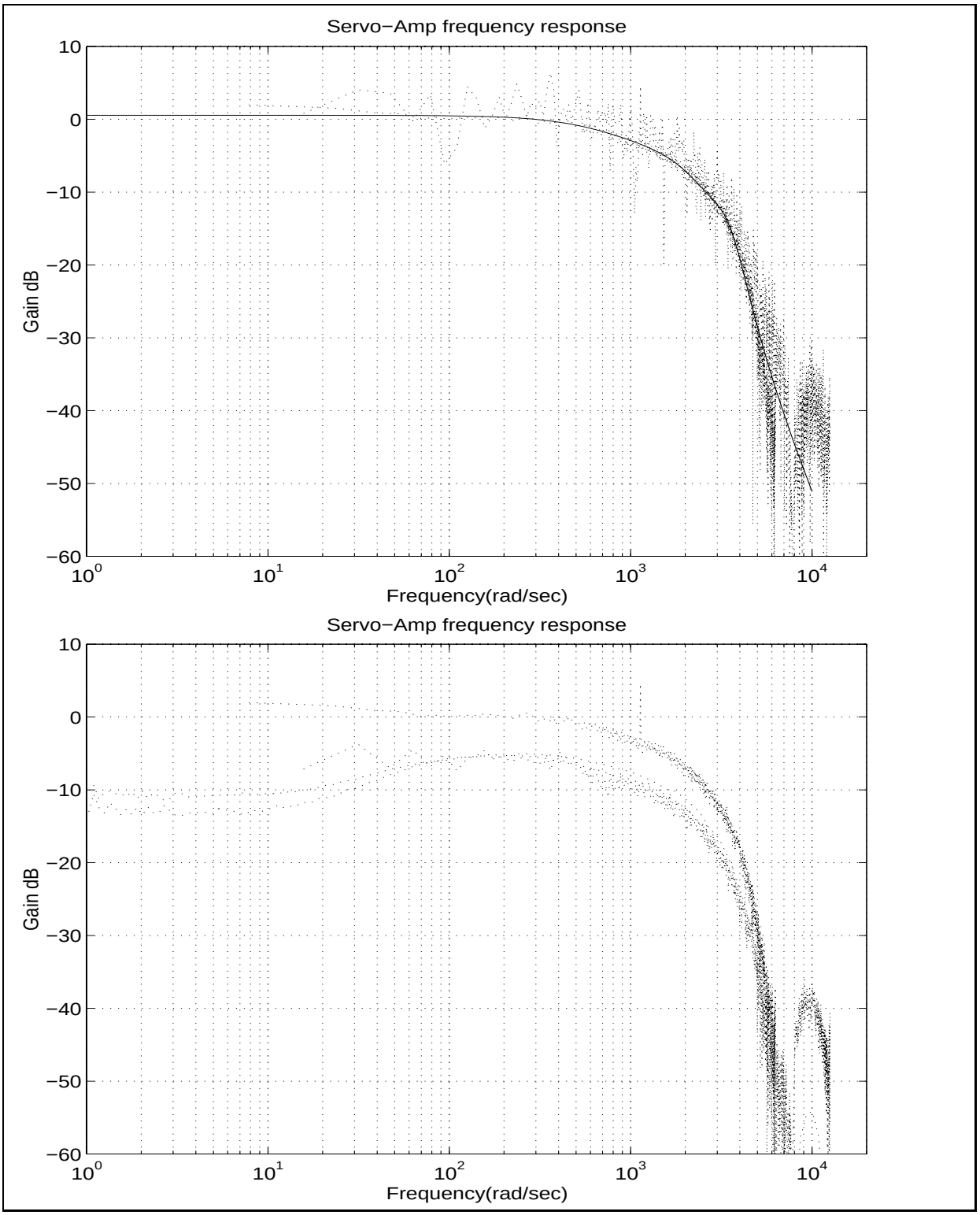

Figure 5: Frequency response of the servo amplifier; Top : Locked load system; Bot : Free load system

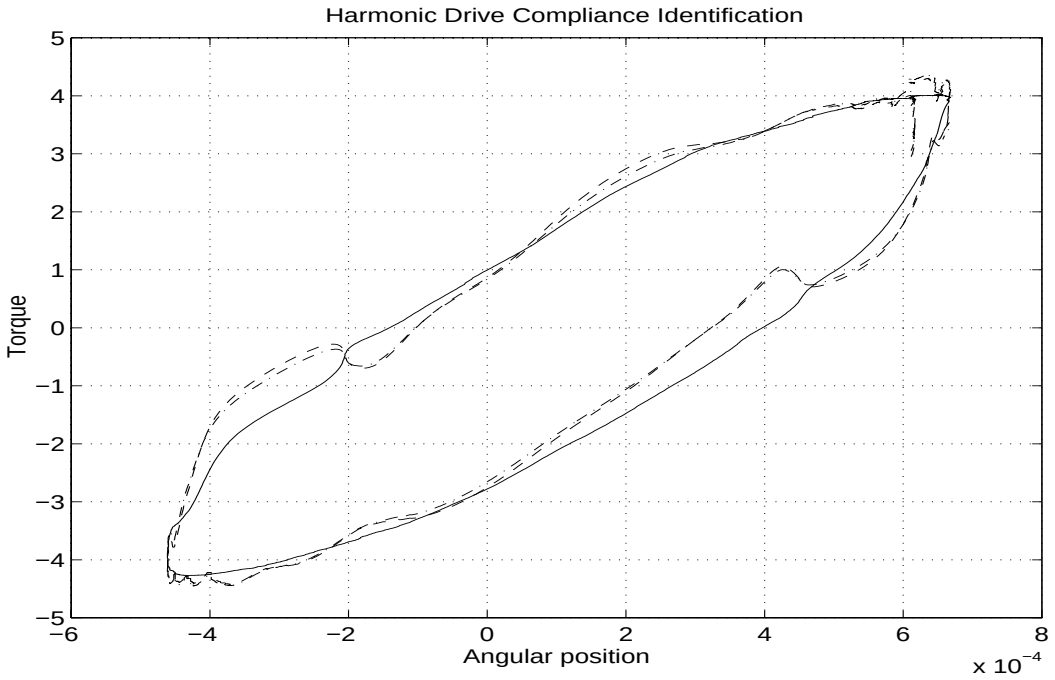

Figure 6: Typical hysteresis curve of the flexspline and its model for optimal α (dash-dot), and $\alpha = \frac{1}{2}$ (dashed)

3.3 Harmonic Drive Characteristics

Harmonic drive transmission is an unconventional gear transmission, which transmits the torque through an elastic element, namely flexspline. This elasticity introduces high flexibility, resonance, and friction losses which are different in nature than that in a conventional gear transmission. Different individual researchers [19, 24, 26, 30], attempted to model and identify harmonic drive by careful static and dynamic experiments. Their experiment were focused to model and identify the stiffness, and friction separately, however as some researchers reported [30], due to inherent coupling of stiffness and friction of the flexspline, the stiffness parameters are not accurately estimated. To avoid this problem we propose to identify the stiffness and damping of the flexspline together for different dynamic experiment by least square approximation. The next section will elaborate this idea.

3.3.1 Compliance

As described in manufacturers' catalogue [20], and as observed by us, a typical shape of the harmonic drive compliance curve can be given by Figure 6. This curve illustrates harmonic drive nonlinear stiffness and hysteresis. To capture the nonlinear stiffness behavior, manufacturers suggest using piecewise linear approximations [20], whereas other researchers prefer a cubic polynomial approximation [31, 32]. The hysteresis effect, however, is more difficult to model, and consequently it is often ignored. Recently Seyfferth et al. proposed a fairly complex model to capture the hysteresis [27]. The hysteresis in the harmonic drive compliance profile may be explained by structural damping of the flexspline. The inherent coupling of stiffness torque and structural damping, therefore, make it very hard to identify those separately. We suggest that Figure 6 is in fact a

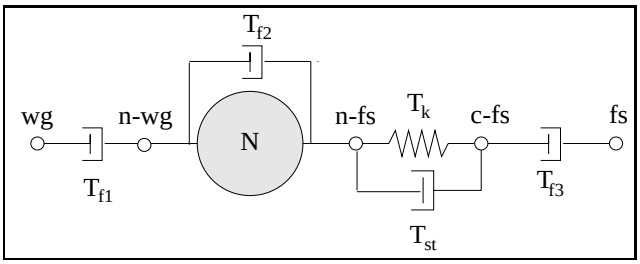

Figure 7: Transmission model of harmonic drive with compliance and friction

Lissajous figure, and we identify both the stiffness and damping of the flexspline together using least square estimation. Linear and cubic models for compliance and many different models for structural damping were tried in this framework. Dahl model for friction [12, 28], Duham, Preisach and Babuska models for hysteresis [25], are among the dynamic models tried to replicate the hysteresis torsion curve. We observed, however, that a linear stiffness model with a static model, relating the structural damping to a power of the velocity can best capture hysteresis behavior of harmonic drive compliance. Equation 5 gives in detail the compliance model, where $\Delta\theta$ is the flexspline relative torsion.

$$T_{meas} = K_1 \Delta\theta + T_{st} |\Delta\dot{\theta}|^{\alpha} \text{sign}(\Delta\dot{\theta}) \tag{5}$$

To identify the model parameters, a set of free load motion experiments has been employed, in which the torque T_{meas} and the motor velocity has been measured. Equation 5 forms a nonlinear regression in which K_1, T_{st} and α are unknown. Using an iterative least square solution for this nonlinear regression model, it is found that the optimal estimate of α is very close to 0.5. Consequently the damping torque of the system can be related to the square root of the relative torsion velocity. Figure 6 illustrates a typical hysteresis torsion curve fitted by the model, comparing the difference between the optimal α and $\alpha = \frac{1}{2}$. By fixing the value of $\alpha = \frac{1}{2}$, Equation 5 forms a linear regression model for the system, that can be solved for different experiments. Table 4 summarizes the compliance parameter of the harmonic drive obtained from more than 20 experiments. The Matlab file stiff–ls.m in Appendix A gives the details of the estimation process.

3.3.2 Friction

All harmonic drives exhibit power loss during operation due to transmission friction. Figure 7 illustrates the schematics of the harmonic drive model. The bulk of energy dissipation can be blamed on the wave generator bearing friction T_{f_1}, gear meshing friction T_{f_2}, output bearing frictions T_{f_3} and flexspline structural damping T_{st}. Among them, most of the frictional dissipation results from gear meshing. Also comparing the ball bearing frictions, T_{f1} is more important than T_{f_3} since it is acting on the high speed/low torque port of transmission, and its effect on the dynamics of the system is magnified by the gear ratio. The transmission torque is measured on the flexspline (namely node c_{fs} of Figure 7). The torque balance, therefore, can be written as:

$$T_{wg} = \frac{1}{N}(T_{meas}) + T_{f_1} + T_{f_2} \tag{6}$$

in which the measured torque $T_{meas} = T_k + T_{st}$, N is the gear ratio, and T_{wg} is the resulting torque of wave generator, provided by the DC–motor. From Equation 1, T_{wg} can be related to the input current by:

$$T_{wg} = K_m i - J_m \ddot{\theta} - T_{f_m} \tag{7}$$

	Estimated Parameter	Consistency Measure
α	$\frac{1}{2}$	0%
K_1	104.2	4.36%
T_{st}	7.96	28.0%
J_{eff}	1.09×10^{-4}	8.72%
T_{v_p}	1.86×10^{-3}	13.2%
T_{v_n}	2.19×10^{-3}	8.42%
T_{s_p}	7.50×10^{-2}	29.2%
T_{s_n}	3.36×10^{-2}	30.8%
$T_{ss_{p1}}$	-4.87×10^{-2}	20.3%
$T_{ss_{n1}}$	-4.50×10^{-2}	18.6%
T_{ss_2}	0.1	0%

Table 4: Harmonic drive estimated parameters

Thus, the final torque balance of the system is the following:

$$K_m i - \frac{1}{N} T_{meas} = J_{eff} \ddot{\theta}_{wg} + (T_{f_m} + T_{f_1} + T_{f_2}) \tag{8}$$

in which K_m is the motor torque constant, J_{eff} is the effective input inertia, and T_{f_m} is the motor friction. The gear meshing friction torque is modelled as Coulomb, viscous and Stribeck friction [5, 29], having velocity direction dependent coefficient as follows:

$$\begin{aligned} T_{f_2} \;=\; & T_{v_p}\dot{\theta}_{wg}\; u_{-1}(\dot{\theta}_{wg}) + T_{v_n}\dot{\theta}_{wg}\; u_{-1}(-\dot{\theta}_{wg}) + \\ & T_{s_p}\mathrm{sign}(\dot{\theta}_{wg})\; u_{-1}(\dot{\theta}_{wg}) + T_{s_n}\mathrm{sign}(\dot{\theta}_{wg})\; u_{-1}(-\dot{\theta}_{wg}) + \\ & T_{ss_{p1}}\mathrm{sign}(\dot{\theta}_{wg})\; u_{-1}(\dot{\theta}_{wg}) e^{-\left(\frac{\dot{\theta}_{wg}}{T_{ss_{p2}}}\right)^2} + T_{ss_{n1}}\mathrm{sign}(\dot{\theta}_{wg})\; u_{-1}(-\dot{\theta}_{wg}) e^{-\left(\frac{\dot{\theta}_{wg}}{T_{ss_{n2}}}\right)^2} \end{aligned} \tag{9}$$

The Stribeck model for friction can capture the dynamics of the friction at low velocities. Unlike compliance identification, both locked load and free load experiments are employed to identify the friction model parameters. Locked load experiments are persistently exciting for viscous and Coulomb friction, while free load experiments operate the system at low velocities which is ideal for Stribeck coefficient identification. Free load low velocity experiments are used as well, for Stribeck coefficient identification. Equation 8 forms a linear regression model for the high velocity experiments in the absence of the nonlinear Stribeck terms. It should be noted that in this regression model instead of the internal system friction T_{f_m}, T_{f_1} and T_{f_2}, the entire friction of the system ($T_f = T_{f_m} + T_{f_1} + T_{f_2}$), can be identified. This imposes no limitation on the identification procedure, since only the entire friction T_f is required for the simulations. For low velocity experiment also, Equation 8 can provide a linear regression if T_{ss_2} is assumed to be known. Figure 8 illustrates the torque fit obtained for four typical experiments. Table 4 summarizes the estimate friction parameters of the harmonic drive assuming fixed $T_{ss_2} = 0.1$, and their consistency measure obtained from more than 25 experiments. The parameters are expressed in SI units. The consistency measure for all parameters are less than 30%, which indicates the reliability of the estimated parameters. It is important to note that the estimated Stribeck friction coefficients are negative, which is in contrary to the usual dynamics of friction reported at low velocities [4, 17]. However, this illustrates

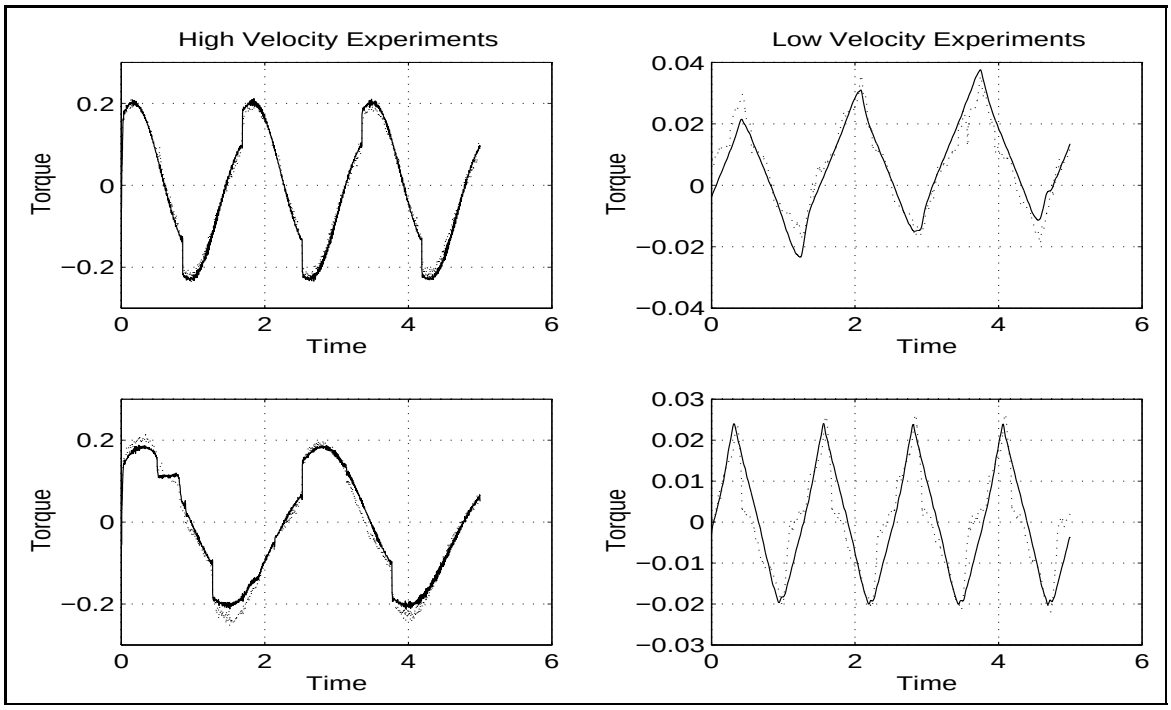

Figure 8: Comparison of model and experiments; dotted: experiment, solid: modelled

that there is no stiction in the harmonic drive transmission, verifying the manufacturers claim [11], nevertheless, it represents exponential rising friction at low velocities. The Matlab files to estimate the friction parameters, fri–in–ls.m and fri–in–nlin.m, are given in Appendix A.

4 Simulations

4.1 Model Verification

To verify the model fidelity, simulations of the system for both locked load and free load systems is developed in Simulink. Figures 9 and 10 illustrate the block diagram of the locked load and free load systems respectively. In both simulation the internal simulation blocks of DC–motor and harmonic drive are shown separately. Different scopes are considered to monitor the signals on line during the simulation. Also the important signals are logged into Matlab workspace for further processing. The simulation input is the measured current experimented on the setup, and therefore, the simulation velocity and torque can be compared to the experiment results. To run the simulation first you should double click on "Load Data" block in the main simulation module. This will automatically compile initialization file and you will see the prompt "Start the simulation now!" in the Matlab workspace. By Choosing "Start" from the simulation menu you can run the simulation, and monitor the desired signal on line on the scopes. After simulation termination, you can double click on "Plot Results" block to see the simulation and experiment velocity and torque comparison automatically. The source files for the simulations are ver–lock.m and ver–free.m, while the initialization files are lock–init.m and free–init.m, and the plotting files are ver–plot.m and free–plot.m. The internal S–functions in the simulation are written in the C language and complied with Cmex compiler to speed up the simulations. The source codes of all the functions are gives in

Appendix A.

Figure 11 illustrates simulation verification results for locked load and free load system for two typical experiments. For locked load case, the match between velocities and torques are quite accurate. Since the velocity for locked load case is relatively small the signal to noise ratio will be larger than the free load case and we have plotted the filtered velocity signals. In free load case, there is very good match for the velocity, and relatively good match for torque curves. Notice that the torque in the free load case are relatively low and there are torque ripples due to the teeth engagement. The model is not capable of exactly replicating this behavior, since the teeth engagement are not modelled in detail. However the overall torque trend is well estimated by the simulations. This was verified for more than fifty other experiments which show a similar match between experiment and simulation. These plots are given in Appendix B. The relatively accurate match between simulation and experiment for different operating ranges, indicates the fidelity of the model to accurately replicate the dynamic behavior of the system.

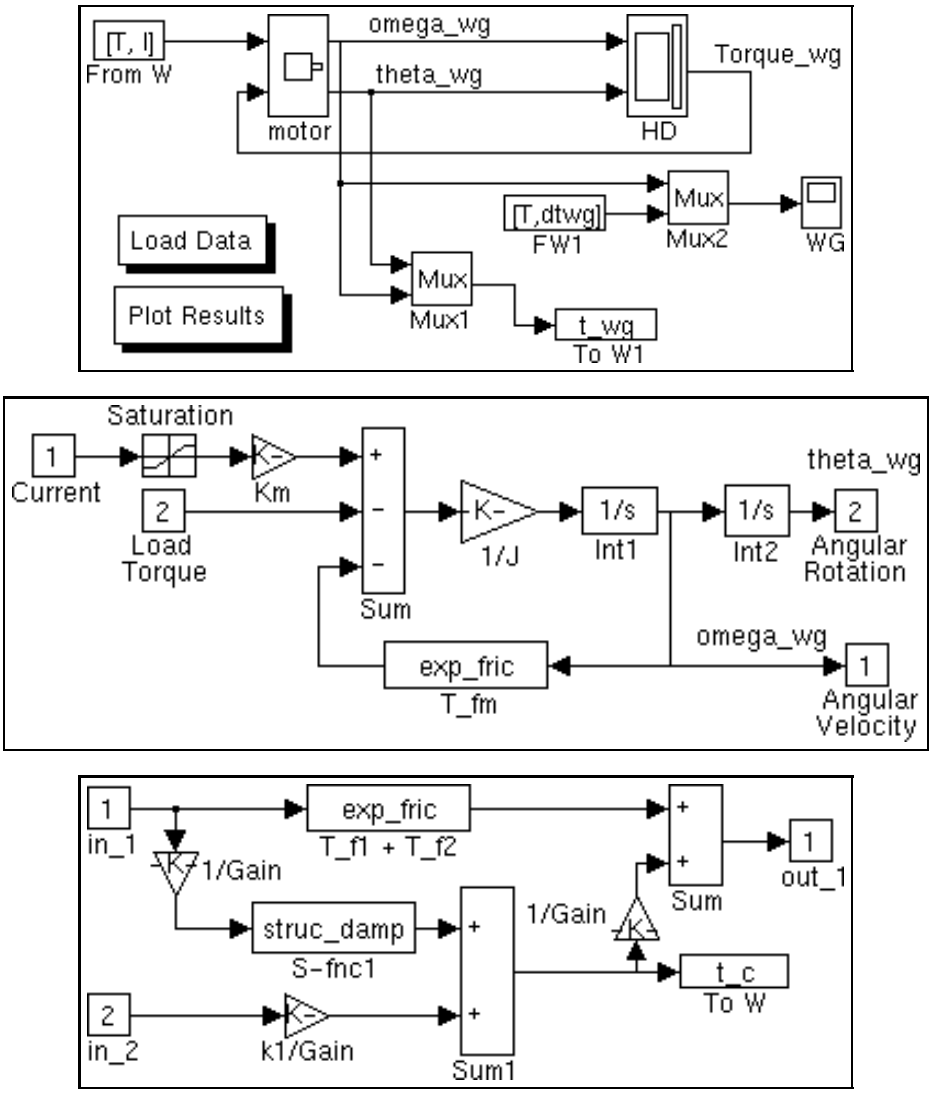

Figure 9: Locked load system simulated on Simulink for model verification purpose. Top: System; Mid: DC–motor; Bot: Harmonic drive

4.2 Locked Load Simulations

A separate simulation for locked load system is developed in Simulink and is illustrated in Figure 12. The reference input to the system is produced using a signal generator. The servo amplifier simple model, namely a constant DC–gain is added into the motor simulation block, but the harmonic drive simulation block is identical to that on Figure 10. The method of running the simulation is quite similar to what explained in Section 4.1; however, the initialization file is sim–lock–init.m, and the plotting file is sim–lock–plot.m. The source codes of these files are given in Appendix A. It is possible to change the input command and monitor the output either online by the scopes or off line on the Matlab workspace. A typical simulation result is illustrated in Figure 12 for a sinusoid input. This module can be further used to include any feedback algorithm, and to evaluate the closed loop system performance in simulations. Notice that the minimum integration period should be smaller than $1ms$ to obtain accurate results.

4.3 Free Load Simulations

Similar to the Locked load simulation module, a separate simulation for free load system is developed in Simulink and is illustrated in Figure 13. A typical simulation result for sinusoid input is also illustrated in Figure 13. The initialization file for this module is sim–free–init.m, and the plotting routine is sim–free–plot.m. The simulation minimum integration time steps should be smaller than $0.1ms$ to obtain accurate results.

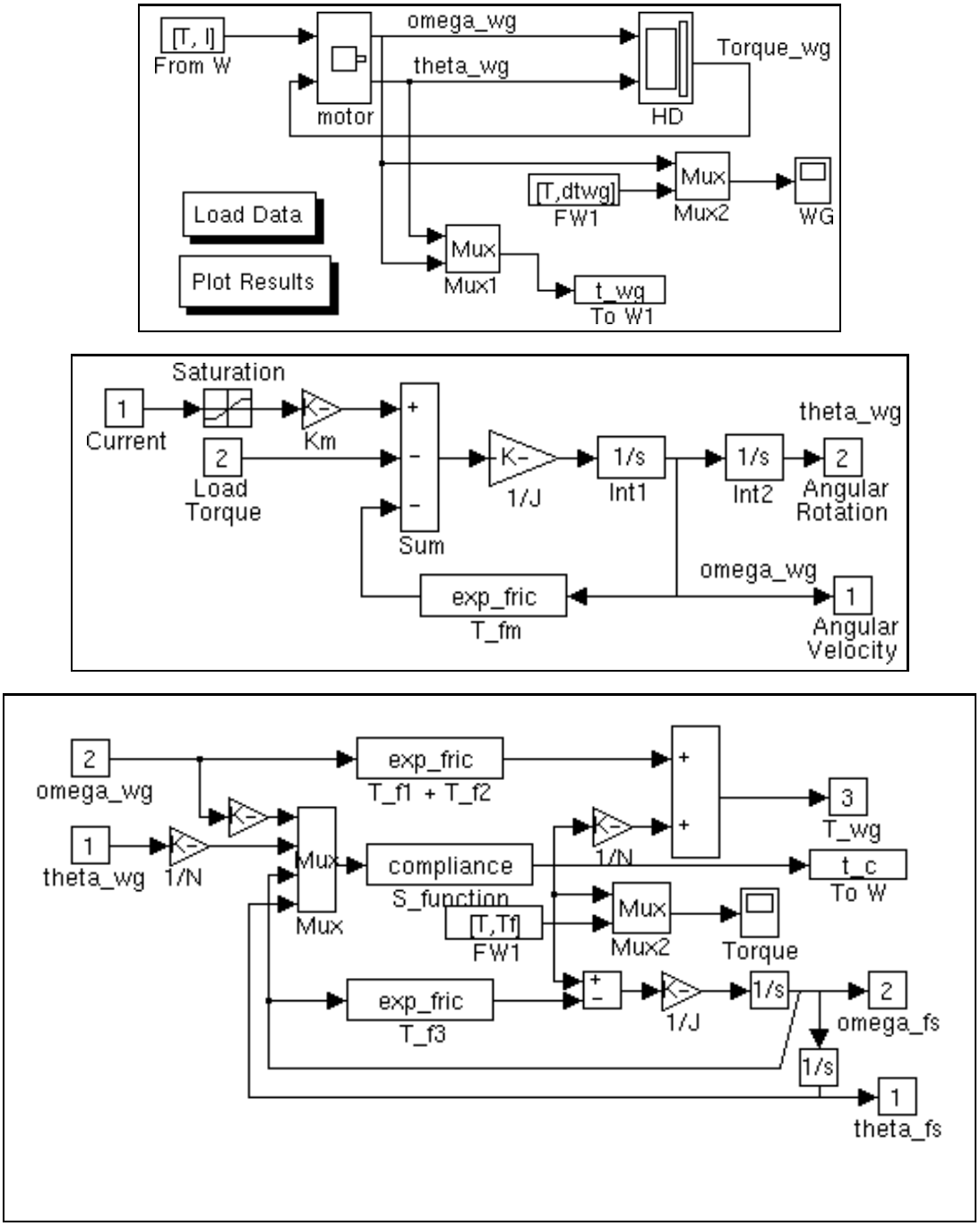

Figure 10: Free load system simulated on Simulink for model verification purpose. Top: System; Mid: DC–motor; Bot: Harmonic drive

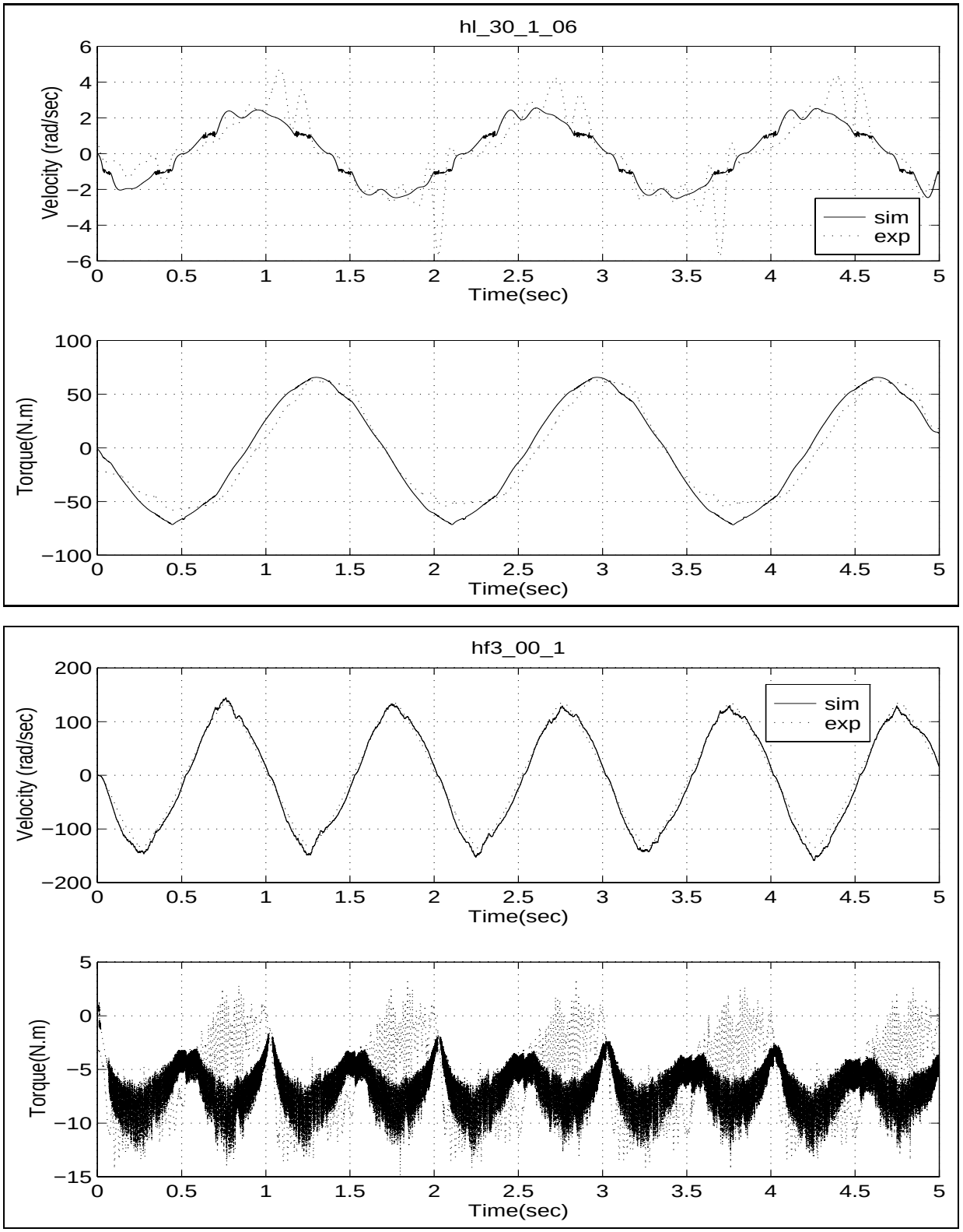

Figure 11: Locked load and Free load simulation verification. Top: Locked load, Bot: Free load

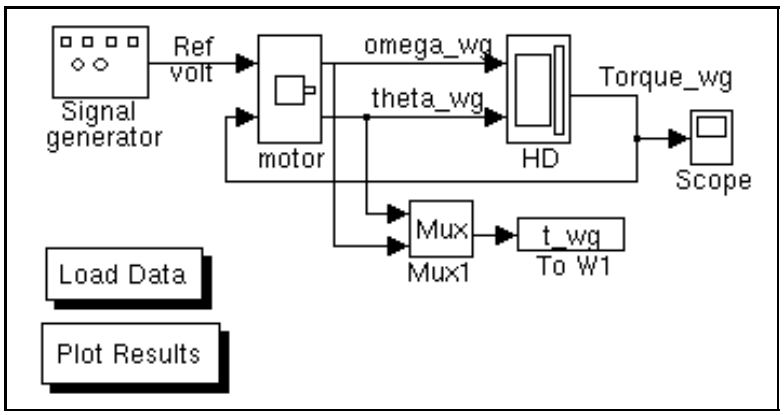

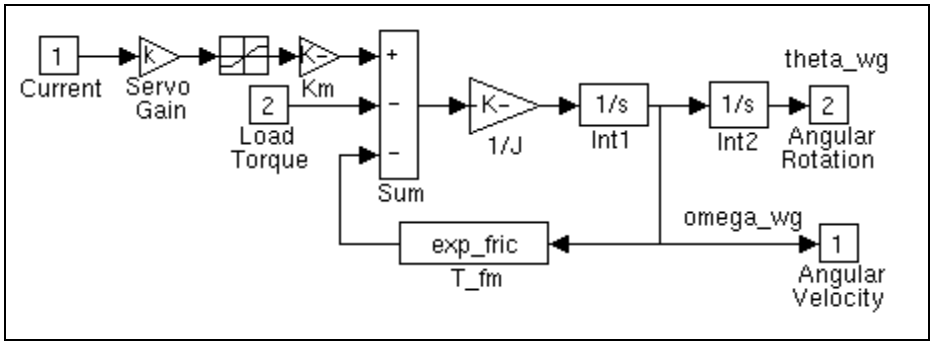

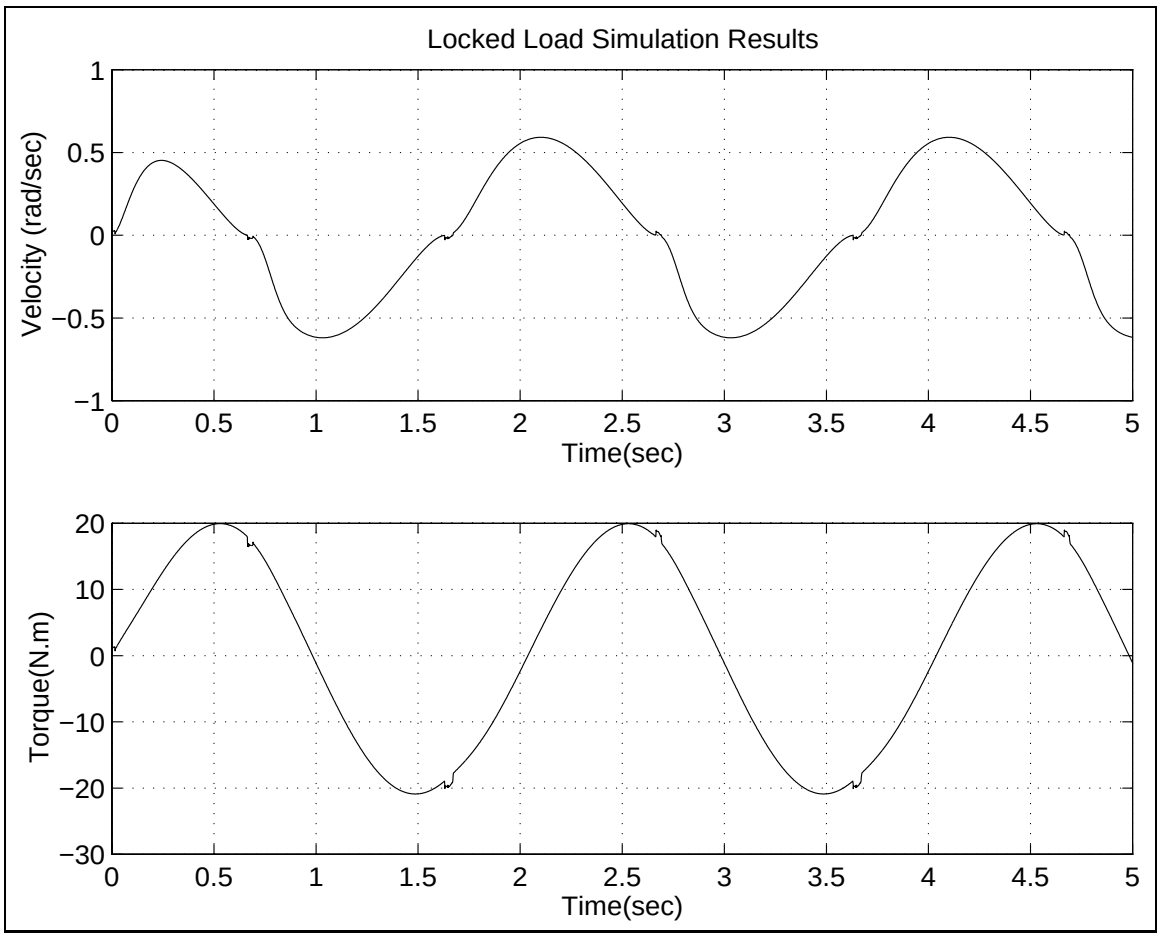

Figure 12: Locked load system simulated on Simulink. Top: system; Mid: DC–motor; Bot: A typical response

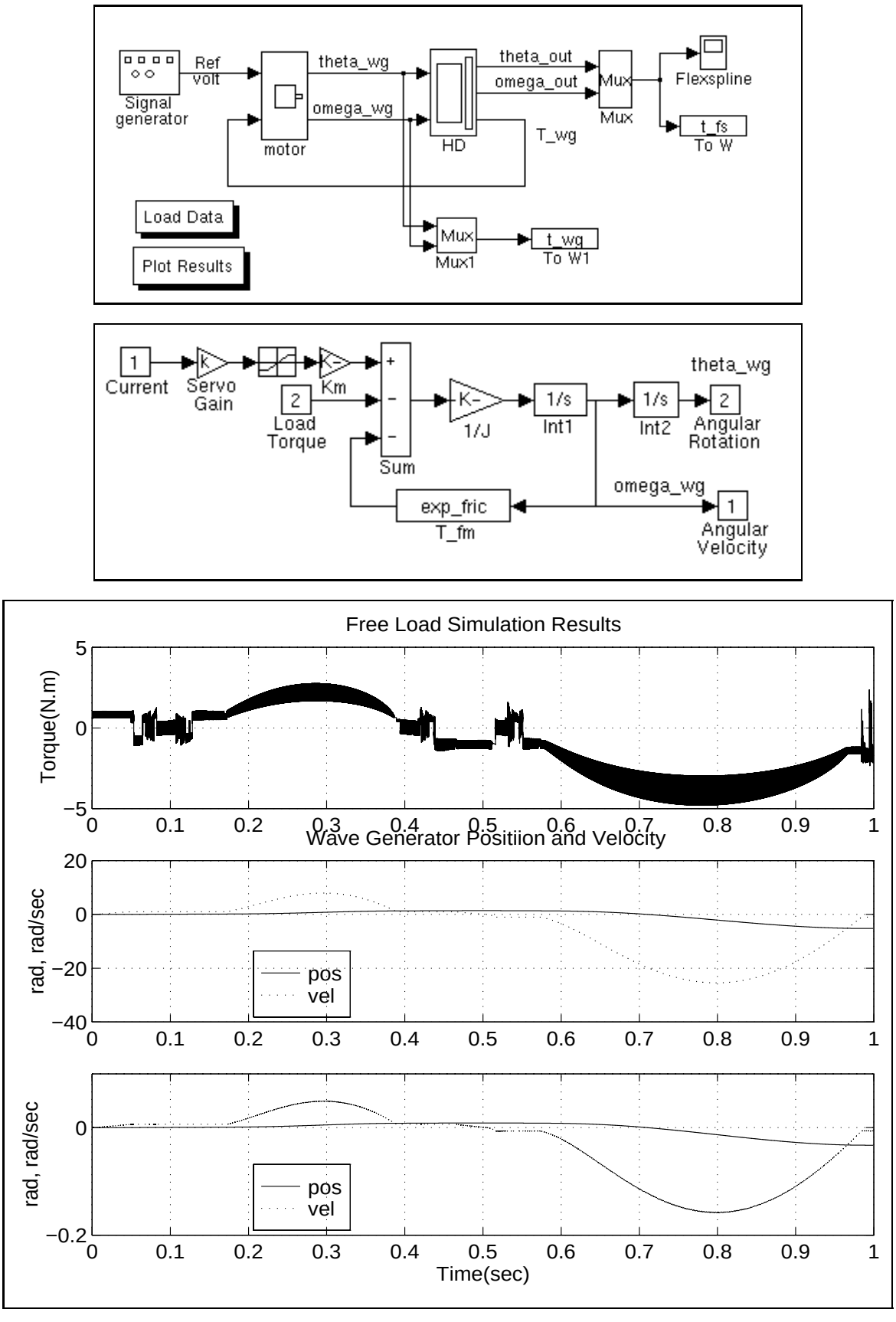

Figure 13: Free load system simulated on Simulink. Top: system; Mid: DC–motor; Bot: A typical response

5 Robust Torque Control

As illustrated in Section 3, to have a relatively accurate model of the system, it is necessary to include hard nonlinear terms like Coulomb friction as well as other type of nonlinearities observed in the structural damping and Stribeck friction. To design a *linear controller*, first a linear model for the system is required, which can be derived by different approaches. The equations of motion of the system can be linearized in a neighbourhood of an equilibrium point [7]. It can be shown that the origin of the state-space is an equilibrium point and the linear model in the vicinity of this equilibrium point is the linear part of the equation of motion. In other words, around this equilibrium point the nonlinearities can be neglected.

In the second method, the system is linearized using feedback. In this method feedback loops are employed to cancel nonlinear terms. Assuming a good knowledge of the system, and a perfect nonlinear dynamic cancellation by feedback, the model of this new system will also include only the linear part of the equation of motion of the original system. The linear model of the system utilizing either of these methods results in a stable second order transfer function, whose frequency response are illustrated in Figure 16 indicated as "Theoretical Model". Another method too find a linear model for the system is to perform a series of frequency response experiments on the system, with different input amplitudes, and to find the best fit through them. By this method not only the empirical nominal model of the system (without need of any linearization) will be determined, but also, the variations in frequency response of system will be encapsulated with an uncertainty representation. Pursuing this method, a transfer function is obtained as the "Nominal Model" of the system, and the upper limit of the frequency response variation is derived using multiplicative uncertainty [15]. Figure 14 illustrates the block diagram of the system using multiplicative uncertainty representation.

The control objective can be defined as *robustly stabilize the system, while maintaining good disturbance attenuation and small tracking error, despite actuator saturation.* More specifically, referring to Figure 14, we would like to design a controller to trade-off minimizing the norm of the transfer function from reference input y_d, to the tracking error e (tracking performance), the transfer function from the disturbance d to the output y (disturbance attenuation), the transfer function from r to q (robust stability), and the transfer function from reference input y_d to the plant input u (actuator limit). This objective is well suited for the general $\mathcal{H}_\infty$ problem.

Figure 15 illustrates the block diagram of the system configured for $\mathcal{H}_\infty$ framework. It can be shown that tracking and disturbance attenuation objectives can be expressed as sensitivity **S** minimization. For multiplicative uncertainty robust stability is guaranteed by a test of the complimentary sensitivity **T** (Small Gain Theorem [33]). **T** can also be shown to be the transfer

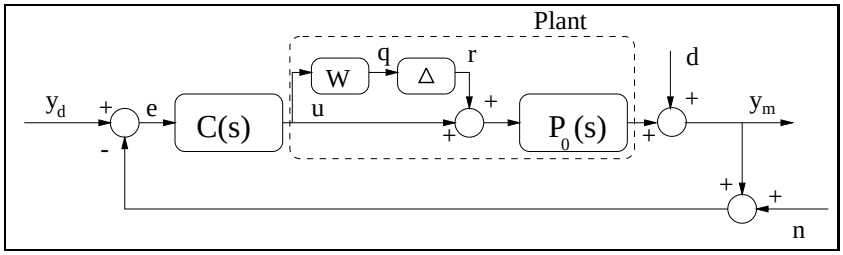

Figure 14: Block diagram of the system considering multiplicative uncertainty for plant

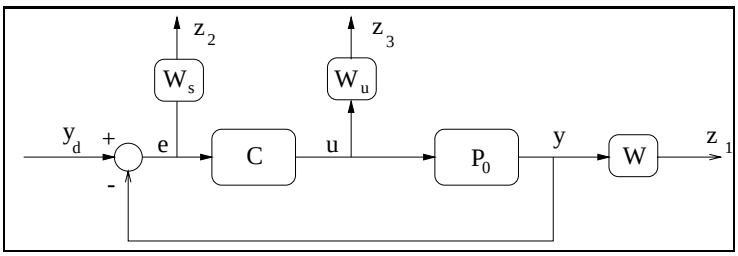

Figure 15: Block diagram of system in the $\mathcal{H}_\infty$framework

function from reference input y_d to the output y [7]. Weighting functions $\mathbf{W}_s$ and $\mathbf{W}_u$ normalize and assign frequency content of the performance objectives on sensitivity and motor current saturation respectively, and $\mathbf{W}$ is the same as multiplicative uncertainty weighting function above. Now the augmented system has one input y_d, and three outputs z_1, z_2, and z_3, in which the transfer function from the input to the outputs corresponds to weighted complimentary sensitivity, weighted sensitivity, and weighted actuator limit respectively. The objectives will now be reduced to finding the controller $C(s)$ which minimizes the infinity norm of the transfer matrix from input y_d to the output vector $\mathbf{z}$ or,

$$\text{Find } C(s) \text{ to minimize } \|\mathbf{T}_{y_d\mathbf{z}}\|_\infty \tag{10}$$

This problem is called a mixed sensitivity problem in literature, and has optimal and suboptimal solution algorithms. Doyle et al. [14], provided the suboptimal solution for this problem in 1989, in which $C(s)$ will be assigned such that $\|\mathbf{T}_{y_d\mathbf{z}}\|_\infty < 1$. The μ-synthesis toolbox of Matlab is uses this algorithm iteratively to find the best suboptimal solution achievable [2].

5.1 Locked Load System

As explained briefly in Section 5, the $\mathcal{H}_\infty$framework for controller design is well suited to the the torque control of harmonic drive. The benefit of using this framework is to have robustness despite nonlinearity in the system. To design a controller we need to provide nominal model of the system, uncertainty representation, desired performance characteristics, and actuator limitations. Figure 16 illustrates the frequency response of the theoretical model, nominal model and a typical experimental frequency response of the system, as well as the uncertainty variations in frequency domain. The transfer function of the theoretical model will simplify to a second order system as follows:

$$\frac{\text{Torque}}{\text{Ref Voltage}} = \frac{\frac{K_{sa}K_1K_m}{K_{ts}NJ_{eff}}}{s^2 + \frac{T_v}{J_{eff}}s + \frac{K_1}{N^2J_{eff}}} \tag{11}$$

where K_{sa} is the DC–gain of the servo amplifier, and K_{ts} is the torque sensor gain. Evaluating the transfer function coefficient by identified parameter given in Table 4, this simplifies to

$$\frac{\text{Torque}}{\text{Ref Voltage}} = \frac{-1.1014 \times 10^4}{s^2 + 18.315s + 5963.827} = \frac{-1.1014 \times 10^4}{s + 9.16 \pm j76.68} \tag{12}$$

The empirical nominal model of the system is found from the best least square fit of the empirical frequency responses of the system and it is also illustrated in Figure 16. The transfer function of the nominal model is also a second order minimum phase transfer function as follows:

$$\frac{\text{Torque}}{\text{Ref Voltage}} = \frac{-9.673 \times 10^3}{s^2 + 142.6s + 7235.2} = \frac{-9.673 \times 10^3}{s + 71.2943 \pm j46.3927} \tag{13}$$

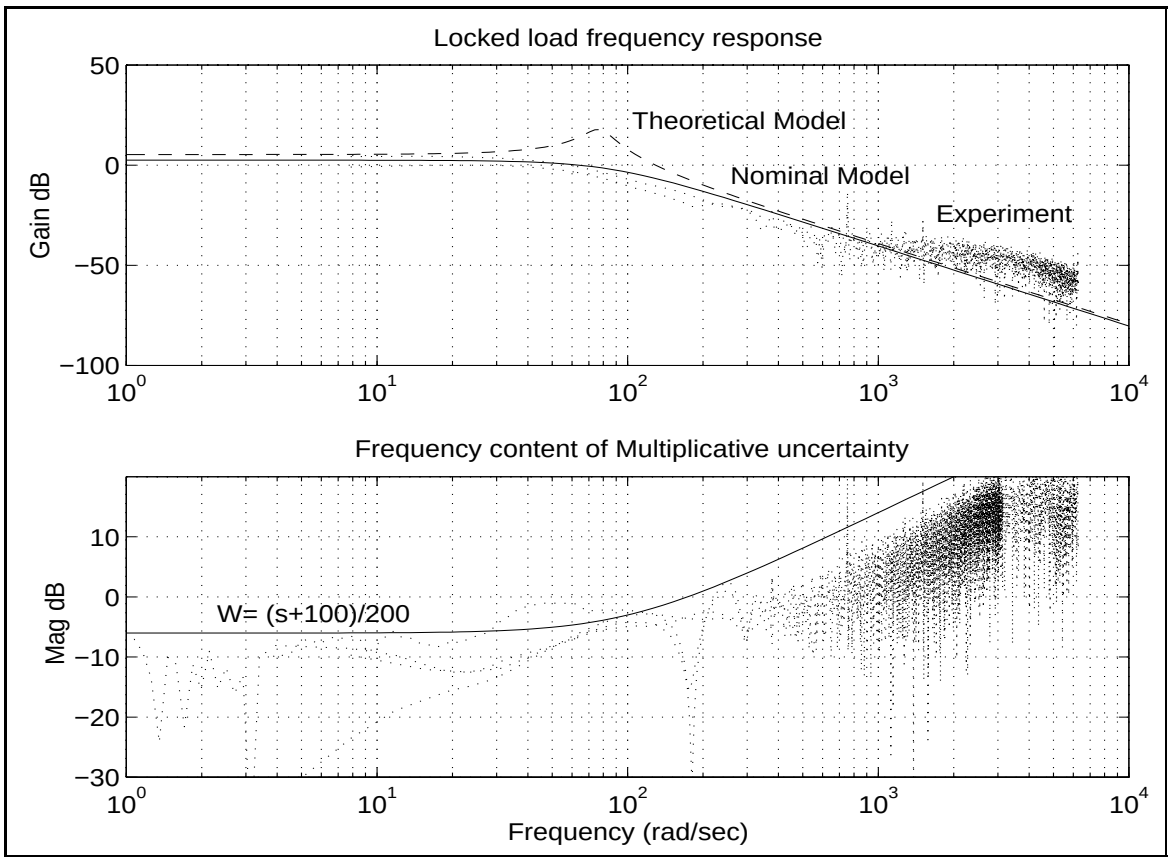

Figure 16: Frequency response of locked load system, theoretical and nominal models, and multiplicative uncertainty

The main difference between the theoretical model and the nominal model is at the resonant frequency, which is due to the cancellation of the nonlinear friction terms in the theoretical model. Therefore, the nominal model and the uncertainty representation of the system is a more accurate representation for controller design.

Assuming multiplicative representation for uncertainty, the uncertainty weighting function which is the upper bound of different uncertainty frequency plots is approximated by $\mathbf{W}(s) = (s + 100)/200$ which is illustrated in Figure 16. Notice that the uncertainty measure at low frequencies is relatively small and about -6 db, which suggest a good match between linear model and the real system within this bandwidth.

Performance weighting functions are selected considering physical limitation of the system. The actuator saturation weighting function is considered to be a constant, by which the maximum expected input amplitude never saturates the actuator. The sensitivity weighting function is assigned to be $\mathbf{W}_s = \frac{s+280}{2(s+2.8)}$. This weighting function indicates that at low frequencies, the closed-loop system should reject disturbance at the output by a factor of 50 to 1. Expressed differently steady-state tracking errors due to step input should be less than 2 % or less. This performance requirement becomes less and less stringent at higher frequencies. For higher frequencies the closed-loop frequency response should degrade gracefully, always lying underneath the inverse of the weighting function $\mathbf{W}_s$. The cut-off frequency for performance is considered 2.8 rad/sec, but could be pushed forward provided the physical limitations of the system, like measurement noise, and actuator saturations

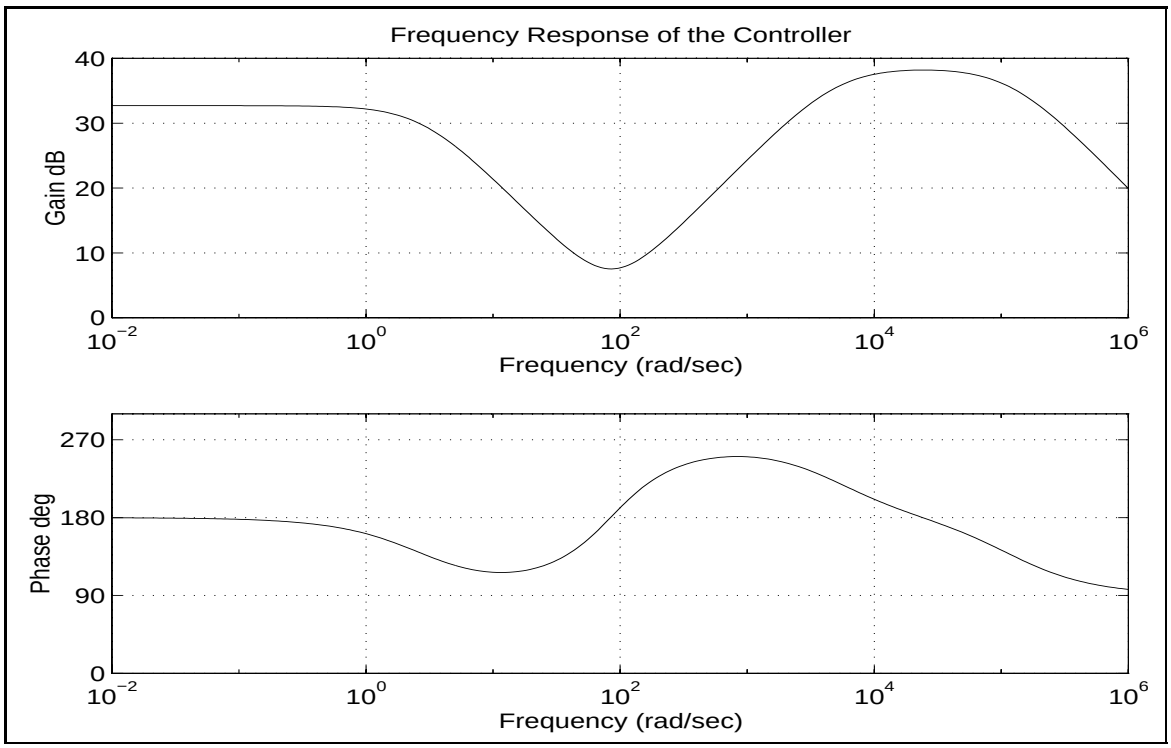

Figure 17: Frequency response of a $\mathcal{H}_\infty$controller designed for locked load system

permit. In practice we can adjust the actuator saturation limit and the performance bandwidth and obtain different controllers. The performance of the controller then can be verified by running some closed loop experiments, and choose the controller with best performance accordingly.

The μ–synthesis toolbox of Matlab is used to design the $\mathcal{H}_\infty$controller. The file hinf–dsg.m, given in Appendix A, is the main program to design the controller, given the plant nominal model and the weighting functions. The program is written in a tutorial format, and by having some knowledge of $\mathcal{H}_\infty$framework the details are understandable. A third order non-minimum phase controller is obtained for the system whose transfer function is:

$$\begin{aligned} K(s) &= \frac{-9.97 \times 10^6 (s^2 + 142.6s + 7235.2)}{s^3 + 1.228 \times 10^5 s^2 + 5.974 \times 10^8 s + 1.672 \times 10^9} \\ &= \frac{-9.97 \times 10^6 (s + 71.2943 \pm j46.3927)}{(s + 2.8)(s + 5972.8)(s + 1.1770 \times 10^5)} \end{aligned} \tag{14}$$

and its frequency response is shown in Figure 17. The order of controller is equal to the order of the augmented system. The controller has two zeros which cancel two stable poles of the system, a pole at the required bandwidth (2.8) and two high frequency poles to shape the sensitivity function at high frequency preserving robust stability in presence of modelling uncertainty. The frequency response of the system especially at the resonance frequency of the system illustrates that the controller has an anti–resonance feature, and since the drop off is not sharp, it is capable of absorbing the possible variations in the resonance frequency.

5.1.1 Controller Performance

To verify the controller performance both simulation and experiments can be utilized. Here we

only report the experimental results which are more convincing. To implement the controller in practice, since we are using computer to realize the controller, bilinear discretization is performed with one kHz sampling frequency. The performance of the closed-loop system can be evaluated in both frequency and time domain.

The frequency domain performance of the closed loop system is illustrated in Figure 19. The closed-loop sensitivity is shown to be underneath the inverse of $\mathbf{W}_s$, as desired, and the phase margin of the system is about 52^o. This is the experimental verification of the $\mathcal{H}_\infty$design claim to preserve robust stability while shaping the performance as desired.

The time domain performance of the system is shown in Figure 20. The tracking of the system for different inputs is illustrated to be very fast and accurate. Although our designed bandwidth is $2.8 rad/sec$, sinusoid inputs up to 10 Hz ($62\ rad/sec$) are shown to be well tracked. Tracking of the system to triangular signal is especially sharp at the edges, and the step response and tracking to an arbitrary signal is shown to be very fast and well-behaved.

In terms of implementation of the controller, it is possible to find a lead–lag controller which best estimates the $\mathcal{H}_\infty$controller. Since the controller is of order three and it has high frequency pole, by cancelling this pole and adjusting for the dc gain, The controller reduces to the following lead–lag transfer function.

$$K(s) = -84.71\frac{s^2 + 1142.6s + 7235}{s^2 + 5076s + 1.42 \times 10^4} = -84.71\frac{(s + 71.2943 \pm j46.3927)}{(s + 2.8)(s + 5972.8)} \tag{15}$$

And it can be realized by the analog circuit illustrated in Figure 18.

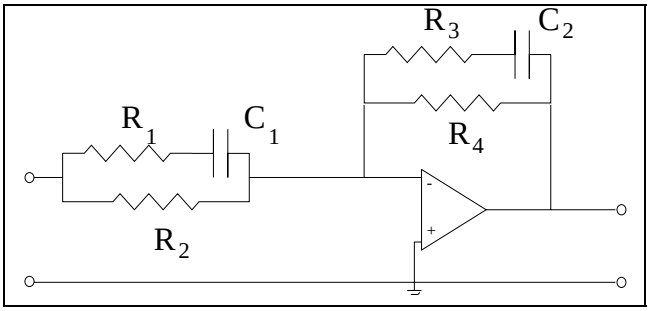

Figure 18: Lead–lag network to realize the controller

5.2 Free Load System

Torque control is historically introduced for the manipulators which are in contact with the environment. For free motions usually a position or velocity feedback suffices to have a desired performance. When a manipulator is in contact with a stiff environment, each joint can be viewed as a locked load system and as shown in last section very good performance can be achieved by torque control techniques. However, when the system is moving freely, the torque delivered by the joint actuators only accelerates the links, and compensates for the friction. The magnitude of the torque delivered in this case is much smaller than that when the robot is in contact with the environment. Also there are three other limitations encountered in free load system.

First the torque is dependent to the acceleration of the output link, therefore the torque and the velocity of the output joint are closely related. Second, the servo amplifier in a free load operating

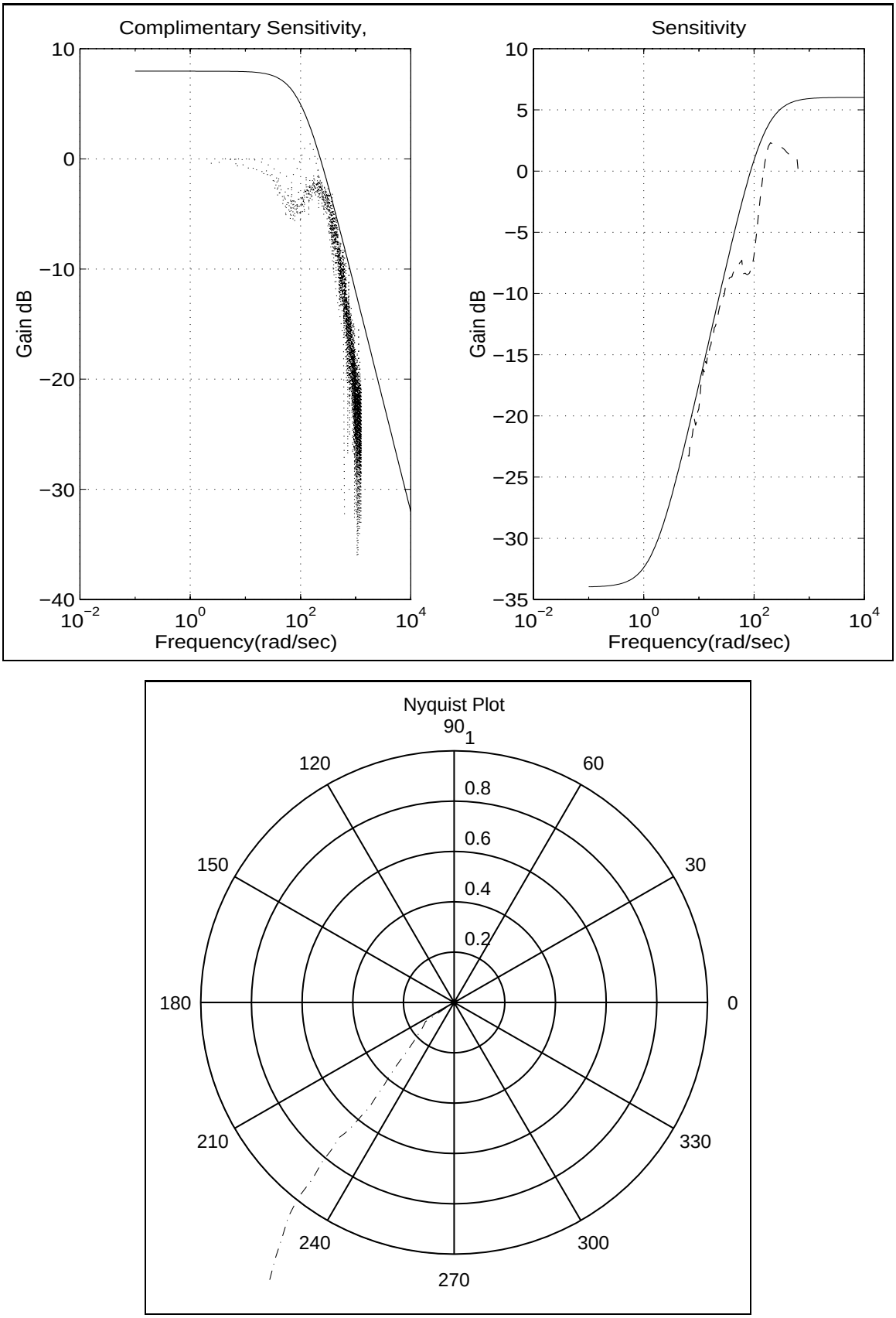

Figure 19: Frequency domain performance characteristics of the closed loop system for locked load case

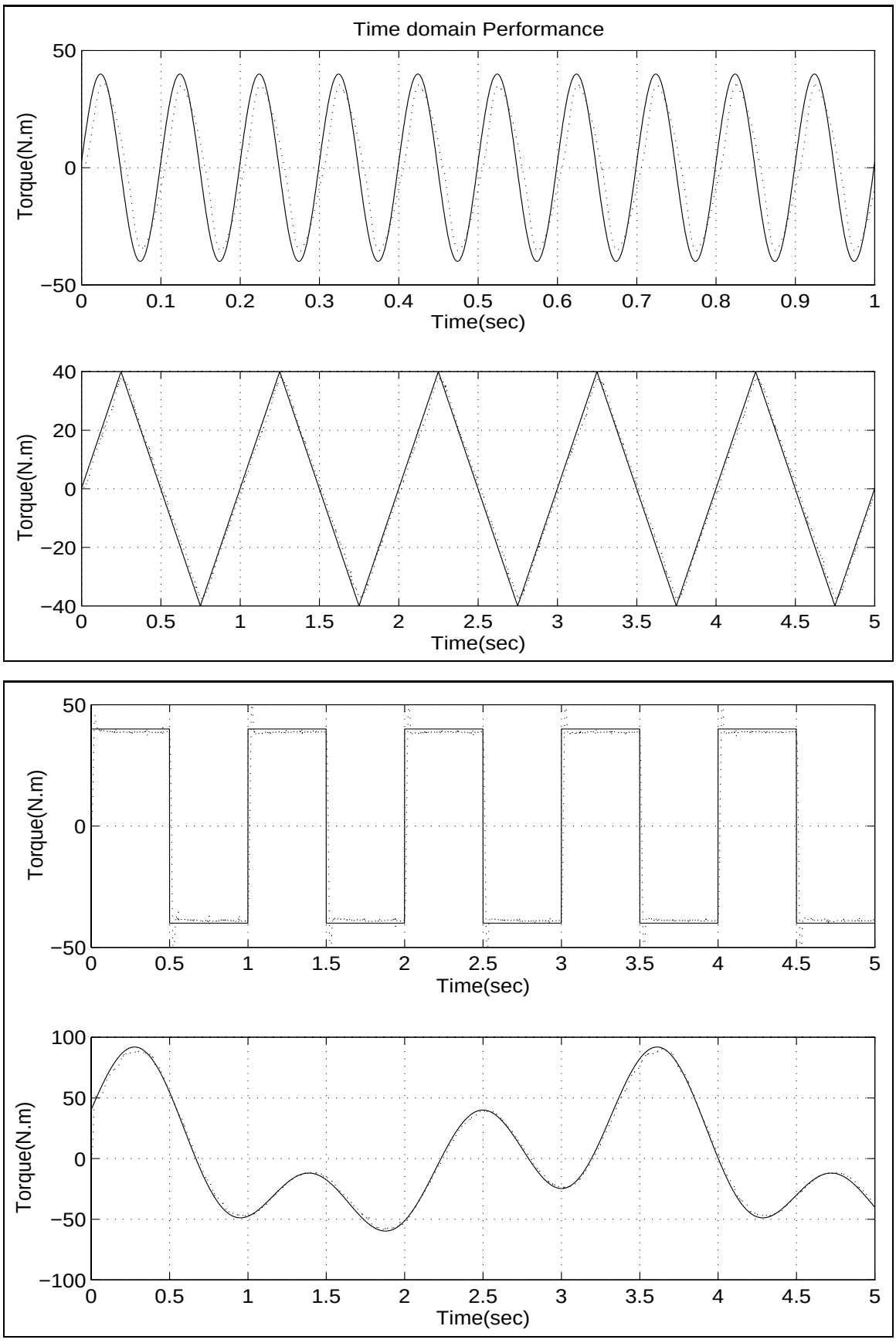

Figure 20: Time domain performance characteristics of the closed loop system for locked load case

condition is not a current source and as illustrated in Figure 5, and explained in Section 3.2, due the the back EMF effect of the motor the servo amplifier looses its DC–gain rapidly relative to the motor speed. Third, each DC–motor has a torque-velocity limit curve, and therefore, the maximum speed of the motor is limited. The combination of this three limitation make it very hard to synthesize a torque source for free load system. To conceptualize the problem consider the simple case of tracking a unit step command. The system will start moving to reach the unit torque, but the output torque is proportional to the acceleration. This means that the system requires a constant acceleration to reach to the desired torque. But this will be interrupted in very short time after the motor reaches its maximum velocity. At this point, no matter how large is the error signal, or how high gain is the controller, the motor will not be able to reach to a higher speed, and therefore to a higher torque. However, if there is any source of external torque applied on the system, like some contact to a stiff environment, the output torque will be not proportional to the output acceleration, and we can reach a desired performance by a torque control method.

To illustrate this limitation, a similar approach to the locked load system has been proposed and some controller have been designed using $\mathcal{H}_\infty$framework. The time domain performance of one of the controller is illustrated in Figure 21 for sinusoid and triangular reference input. It is shown that when the reference torque is small enough to move the system at very low velocities, the desired torque is tracked fairly well. However, the tracking ability degrades when the system starts moving freely by nominal speeds. This result confirms the inherent difficulty producing a torque source for the free load system, and suggest that velocity feedback is preferable for this case.

6 Conclusions

Based on experimental and theoretical studies, a systematic way to capture and rationalize the dynamics of harmonic drive systems is introduced. Simple and accurate models for compliance, hysteresis, and friction are established and model parameters are identified using least square approximation. A measure of consistency is defined, by which the reliability of the estimated parameter over different operating conditions, as well as the accuracy of the model is quantified. From compliance modelling results, it has been illustrated that identifying stiffness and structural damping together will resolve the reported difficulties in determining the compliance parameters. Moreover, it has been shown that a linear stiffness model best captures the behavior of the system when combined with a good model for hysteresis. A simple static model for hysteresis is also introduced, and it is shown that this simple model can replicate the hysteresis effect in harmonic drives better than most other dynamic models reported in the literature. Friction losses of the harmonic drive are modelled at both low and high velocity operating regimes. From experiments on the harmonic drive system it has been observed that there is no stiction in the transmission, but rather an exponential rising friction at low velocities. The model performance is assessed by two simulation built in Simulink, verifying the experimental results for both locked load and free load systems.

The problem of torque control of harmonic drive is addressed in the $\mathcal{H}_\infty$controller design framework. An empirical linear model for the system, and a measure of the uncertainty of that model are estimated from experimental frequency responses of the system. It has been shown that this model and its multiplicative uncertainty representation provides necessary requirements for controller design. It is illustrated that the $\mathcal{H}_\infty$framework is a very powerful theory to ensure the stability and performance requirements in presence of modelling uncertainties. The designed con-

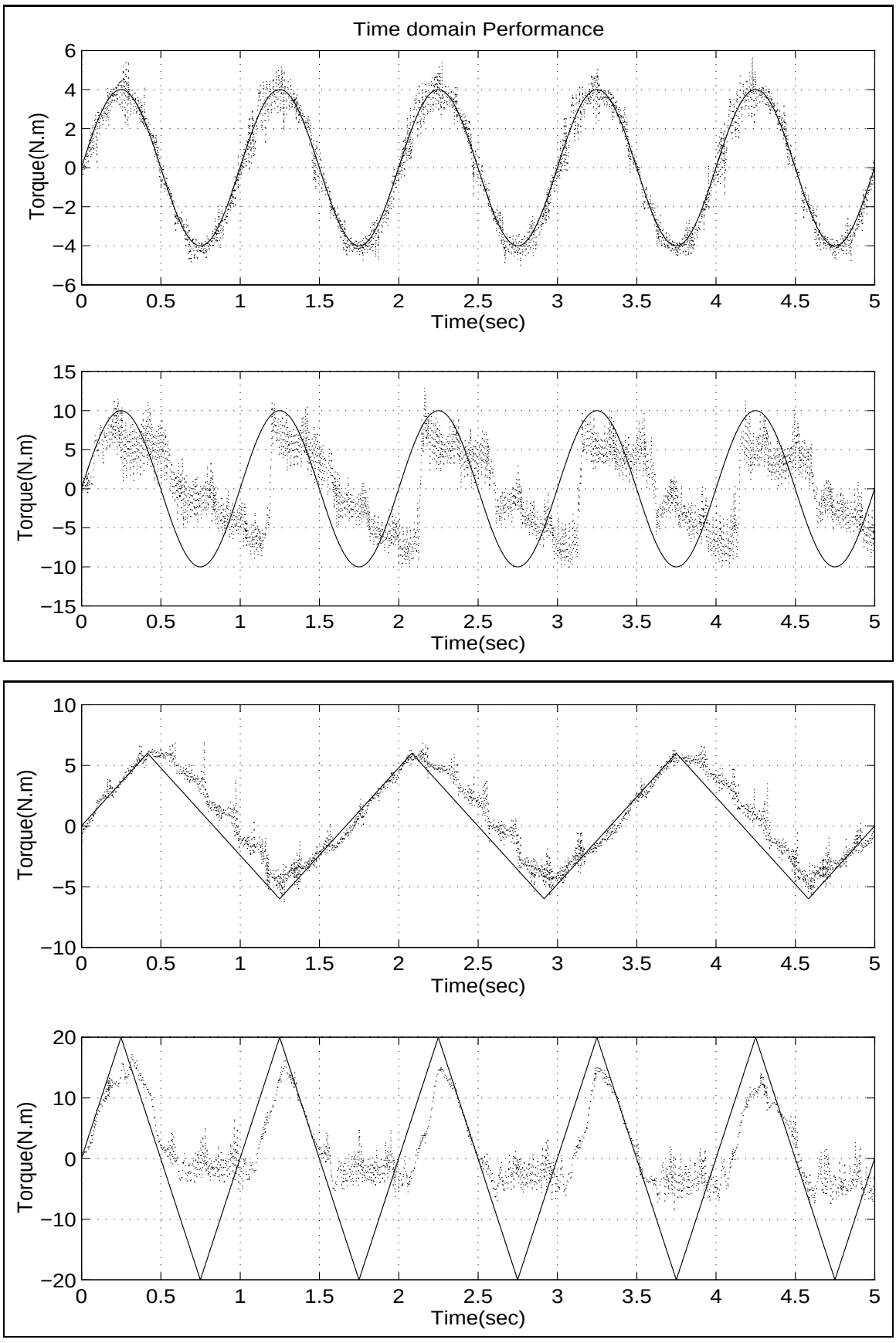

Figure 21: Time domain performance characteristics for the closed loop system for free load case

troller are shown to be easily implementable with either computer controlled method or with an analog lead-lag network. Finally, the performance of the closed loop system in time and frequency domain are shown to be exceptionally good.

There are numerous future research opportunities to improve the modelling and controller design for harmonic drive systems. In terms of modelling, detailed model for the gear meshing mechanism can improve the simulation results in a free load case. The rippling of output torque is not accurately estimated by the present representation. However, the torque control scheme implemented on the harmonic drive, illustrates that to design a controller only a linear empirical model of the system suffice for good performance. Thus, for torque control applications it is not necessary to model the system to that detail. In terms of control, there are two different horizons of improvements. In locked load case, the issue of output noise and its effect on the system performance were not addressed theoretically in controller design. This factor combined with the actuator saturation, limits the bandwidth of the closed loop system. However, the $\mathcal{H}_\infty$framework is capable of including the effect of output noise in the performance. In the free load case the inherent difficulties of the system to develop a torque source were illustrated. However, alternative ideas such as impedance or hybrid control can be examined.

References

[1] *DSP Technology Inc. Siglab Version 1.0.*

[2] *Mu Analysis and Synthesis Toolbox.*

[3] N.A. Aliev. A study of the dynamic behavior of flexible gears in harmonic drives. *Soviet Engineering Research*, 66(6):7–11, 1986.

[4] B. Armstrong-Helouvry. Stick slip and control in low speed motion. *IEEE Transactions on Automatic Control*, 38(10):1483–1496, October 1993.

[5] B. Armstrong-Helouvry, P. Dupont, and C. Canudas de Wit. A survey of models, analysis tools and compensation methods for control of machines with friction. *Automatica*, 30(7):1083–1138, 1994.

[6] P.R. Bélanger. Estimation of angular velocity and acceleration from shaft encoder measurements. Technical Report TR-CIM-91-1, Center for Intelligent Machines, 1991.

[7] P.R. Bélanger. *Control Engineering, A Modern Approach.* Saunders College Publishing, 6277 Sea Harbour Drive, Orlando, Florida 32887-6777, 1995.

[8] A. Ben-Israel. *Generalized Inverses: Theory and Application.* Wiley, New York, 1974.

[9] M.M. Bridges, D.M. Dawson, and S.C. Martindale. Experimental study of flexible joint robots with harmonic drive gearing. *Proceedings of the IEEE Conference on Control Applications*, 2:499–504, 1993.

[10] J.D. Chapel. Attaining impedance control objectives using H–infinity design methods. *Proceeding of IEEE International Conference on Robotics and Automation*, 2:1482–87, 1991.

[11] J.H. Charlson. Harmonic drives for servomechanisms. *Machine design*, 57(1):102–106, January 1985.

[12] P.R. Dahl. Solid friction damping of mechanical vibration. *AIAA Journal*, 14(12):1675–1682, December 1976.

[13] K.L. Doty, C. Melchiorri, and C. Bonivento. Theory of generalized inverses applied to robotics. *International Journal of Robotics Research*, 12(1):1–19, Feb 1993.

[14] J. Doyle, K. Glover, P.P. Khargonekar, and B. A. Francis. State-space solution to standard H–two and H–infinity control problems. *IEEE Transactions on Automatic Control*, AC-34(8):831–847, 1989.

[15] J.C. Doyle, B.A. Francis, and A.R. Tannenbaum. *Feedback control theory.* Macmillan, N.Y., 1990.

[16] G.H. Golub and C. Van Loan. *Matrix computations.* The Johns Hopkins University Press, Baltimore, MD, 1983.

[17] D.P. Hess and A. Soom. Friction at a lubricated line contact operating at oscillating sliding velocities. *Journal of Tribology*, 112(1):147–152, January 1990.

[18] Neville Hogan. Impedance control of robots with harmonic drive system. *Proceeding of the American Control Conference*, 1:398–402, 1991.

[19] L. Hsia. The analysis and design of harmonic gear drives. *Proceedings of the 1988 IEEE International Conference on Systems, Man and Cybernetics*, 1:616–619, 1988.

[20] HD Systems Inc. Harmonic drive gearing. *HD Systems Catalogue*, 1991.

[21] K. Kaneko, T. Murakami, K. Ohnishi, and K. Komoriya. Torque control with nonlinear compensation for harmonic drive DC motors. *IECON Proceedings*, 2:1022–1027, 1994.

[22] H. Kazerooni. Dynamics and control of instrumented harmonic drives. *Journal of Dynamic Systems Measurement and Control - Transactions of the ASME*, 117(1):15–19, March 1995.

[23] N. Kircanski, A. Goldenberg, and S. Jia. An experimental study of nonlinear stiffness, hysteresis, and friction effects in robot joint with harmonic drives and torque sensors. *Proceedings of the Third International Symposium on Experimental Robotics*, 1:147–154, 1993.

[24] G. legnani and R. Faglia. Harmonic drive transmission: the effect of their elasticity, clearance and irregularity on the dynamic behaviour of an actual SCARA robot. *Robotica*, 10:369–375, October 1992.

[25] J.W. Macki, P. Nistri, and P. Zecca. Mathematical models for hysteresis. *SIAM Review*, 35(1):94–123, March 1993.

[26] T. Marilier and J.A. Richard. Non-linear mechanic and electric behavior of a robot axis with a harmonic-drive gear. *Robotics and Computer-Integrated Manufacturing*, 5(2/3):129–136, 1989.

[27] W. Seyfferth, A.J. Maghzal, and J. Angeles. Nonlinear modelling and parameter identification of harmonic drive robotic transmissions. *Proceeding of IEEE International Conference on Robotics and Automation*, 3:3027–3032, 1995.

[28] D.C. Threlfall. The inclusion of coulomb friction in mechanisms programs with particular reference to DRAM. *Mech. and Mach. Theory*, 13:475–483, 1978.

[29] A. Tustin. The effects of backlash and speed-dependent friction on the stability of closed-cycle control systems. *J. Inst. Elec. Eng.*, 94(2A):143–151, 1947.

[30] T.D. Tuttle. Understanding and modelling the behavior of a harmonic drive gear transmission. Technical Report 1365, MIT Artificial Intelligence Laboratory, 1992.

[31] T.D. Tuttle and W. Seering. Modelling a harmonic drive gear transmission. *Proceeding of IEEE International Conference on Robotics and Automation*, 2:624–629, 1993.

[32] D.P. Volkov and Y.N. Zubkov. Vibration in a drive with harmonic gear transmission. *Russian Engineering Journal*, 58(5):17–21, 1978.

[33] G. Zames. On the input-output stability of time-varying nonlinear feedback systems. *IEEE Transcript on Automatic Control*, II(Part I, and II):228–238, and 465–476, 1966.

A Source Codes

A.1 Matlab Files for Least Square Approximation

tach–ls.m
mot–lin–ls.m
stiff–ls.m
fri–in–ls.m
fri–in–nlin.m
amp–freq–fit.m
lock–freq–fit.m
free–freq–fit.m

A.2 Matlab Files on Simulations

lock–init.m
free–init.m
ver–plot.m
free–plot.m
sim–lock–init.m
sim–free–init.m
sim–lock–plot.m
sim–free–plot.m

A.3 Matlab C Codes for Simulations

exp–fric.c
struct–damp.c
compliance.c

A.4 Matlab Files for $\mathcal{H}_\infty$Design

hinf–dsg.m

B Matlab Plots

B.1 Locked Load Simulation Verification

File name description:
Note that the title of the figures are the experiment filenames. The convention to build the filename is such that the experiment information are included in it. For example in filename hl–30–1–03 the first two letters indicate the harmonic drive experiment in locked load, the two next digits are the amplitude of the reference input, 30 % of the maximum, the next digit illustrates the input shape function, where 1 : Sinusoid, 2 : Square wave, 3 : Triangular. The last two digits represents the frequency, which in this example is 0.3 Hz.

B.2 Free Load Simulation Verification

File name description:
Similar convention is used for the free load experiments, hf1–30–03 with the difference that the input shape function index come first next to the harmonic drive free load experiment notation.

C Experimental Setup Designs Drawings

C.1 Free Load Assembly

C.2 Locked Load Assembly

C.3 Tachometer Assembly

C.4 Torque Sensor Calibration Assembly

D System Component's Technical Specs

D.1 DC–Motor

D.2 Harmonic Drive

D.3 Tachometer

D.4 Encoder